BIOCHEMISTRY
including biophysical chemistry & molecular biology

Article

pubs.acs.org/biochemistry

A Molecular Dynamics Simulation-Based Interpretation of Nuclear Magnetic Resonance Multidimensional Heteronuclear Spectra of α-Synuclein·Dopamine Adducts

Domenica Dibenedetto,[†] Giulia Rossetti,*[,†,‡,§,∥] Rocco Caliandro,[⊥] and Paolo Carloni[†]

[†]Computational Biophysics, German Research School for Simulation Sciences (joint venture of RWTH Aachen University and Forschungszentrum Jülich), D-52425 Jülich, Germany, and Institute for Advanced Simulation IAS-5, Computational Biomedicine, Forschungszentrum Jülich, D-52425 Jülich, Germany

[‡]Institute for Research in Biomedicine (IRB Barcelona), Baldiri Reixac 10, Barcelona 08028, Spain

[§]Joint IRB-BSC Program in Computational Biology, Barcelona, Spain

[∥]John von Neumann Institute for Computing (JSC), Forschungszentrum Jülich, Jülich, Germany

[⊥]Institute of Crystallography (IC), National Research Council of Italy (CNR), via Amendola, 122/o, 70126 Bari, Italy

Supporting Information

ABSTRACT: Multidimensional heteronuclear nuclear magnetic resonance (NMR) spectroscopy provides valuable structural information about adducts between naturally unfolded proteins and their ligands. These are often highly pharmacologically relevant. Unfortunately, the determination of the contributions to observed chemical shifts changes upon ligand binding is complicated. Here we present a tool that uses molecular dynamics (MD) trajectories to help interpret two-dimensional (2D) NMR data. We apply this tool to the naturally unfolded protein human α-synuclein interacting with dopamine, an inhibitor of fibril formation, and with its oxidation products in water solutions. By coupling 2D NMR experiments with MD simulations of the adducts in explicit water, the tool confirms with experimental data that the ligands bind preferentially to ^{125}YEMPS^{129} residues in the C-terminal region and to a few residues of the so-called NAC region consistently. It also suggests that the ligands might cause conformational rearrangements of distal residues located at the N-terminus. Hence, the performed analysis provides a rationale for the observed changes in chemical shifts in terms of direct contacts with the ligand and conformational changes in the protein.

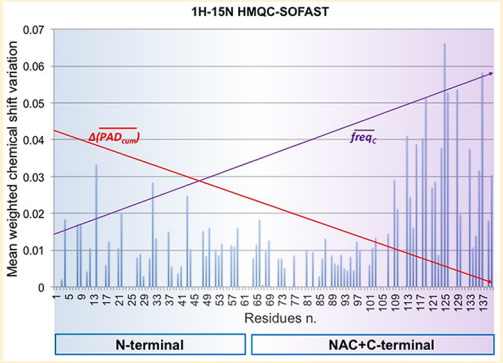

The human α-synuclein protein (AS hereafter)[1−3] is a midsize [140 amino acids (Figure 1A)] intrinsically disordered protein (IDP) involved in Parkinson's disease.[4] The protein forms fibrillar aggregates in the brain (Lewy bodies), characteristic of the disease.[5−7] These fibrils may also mediate the toxicity to dopaminergic neurons in Parkinson's disease pathogenesis and in cell death.[8−10]

Dopamine and its derivatives[11,12] (DOP hereafter) in Figure 1B are known to inhibit AS fibril formation *in vitro* and *in vivo*.[11,13−19] Inhibition of fibrillation may be achieved by noncovalent[a] binding of DOP to the AS C-terminal region specifically targeting the ^{125}YEMPS^{129} region.[13,15,17,18] Recently, two-dimensional (2D) ^{1}H−^{15}N heteronuclear single-quantum correlation (HSQC) spectra of the AS·DOP complex[20] have shown noncovalent binding of DOP at the C-terminus of AS. This binding may play a role in the DOP-induced inhibition of AS fibril formation.[13,15]

2D heteronuclear NMR methods,[21,22] in which ^{1}H nuclei are correlated with ^{15}N,[22] are widely used to investigate structural aspects of intrinsically disordered proteins and their binding with ligands.[20,23] In some cases, these techniques are coupled with paramagnetic relaxation enhancement (PRE) measurements.[24] Heteronuclear multiple-quantum correlation (HMQC) recorded with selective optimized-flip-angle short-transient (SOFAST)[23,25] improves the measured resolution of the spectra.[23,25] Particularly useful are the 2D HMQC and HSQC experiments, which permit the detection of correlations between nuclei of two different types, separated by one bond. It is in general possible to assign heteronuclear chemical shifts even for proteins of up to several hundred amino acids.[26,27]

Unfortunately, interpreting changes in chemical shifts or peak intensities upon ligand binding for IDPs is challenging. In all of these methods, spectral changes can be caused by a variety of contributions. They may arise from conformational transitions associated with long-range effects,[27] chemical exchanges,[21] molecular interactions (including those caused by direct contacts formed between the protein and the ligand),

Received: March 21, 2013
Revised: August 19, 2013
Published: August 21, 2013

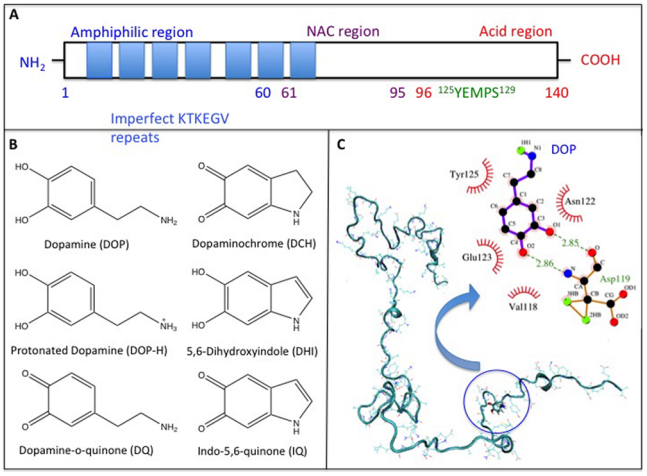

Figure 1. (A) Schematic representation of AS protein. AS consists of 140 amino acids. (i) The positively charged N-terminal region (amino acids 1−60, blue) comprises the seven imperfect 11-amino acid repeats containing the KTKEGV consensus sequence. (ii) The non-β-amyloid component (NAC, violet) comprises amino acids 61−95. (iii) The negatively charged C-terminal region (amino acids 96−140, red) contains several sites of post-translational modification. The ^{125}YEMPS^{129} region is colored green. (B) Dopamine and its derivatives, which may be present *in vivo* and *in vitro*.[11,12] These are protonated dopamine (DOPH), dopamine (DOP), dopamine-*o*-quinone (DQ), dopaminochrome (DCH), 5,6-dihydroxyindole (DHI), and indol-5,6-quinone (IQ). (C) DOP−AS contacts. A molecular dynamics snapshot of DOP noncovalently bound to AS in representative configuration **2** is shown as an example. Both a three-dimensional (3D) representation and an interaction scheme (obtained with Ligplot[79]) are shown. In the 3D representation, the atoms involved in the binding are shown as a combinations of "lines" and "cartoon" representation, while the molecule is shown in "licorice" representation. In the scheme, HBs are indicated by dashed lines between the atoms involved, while HCs are represented by an arc with spokes radiating toward the ligand atoms they contact. The other adducts are reported in Figures S2 and S3 of the Supporting Information.

and possible interactions with weakly populated secondary products of the ligands, which may modify residues' conformations.[28]

Computational methods may be of great help in dissecting the contributions to NMR chemical shifts arising from direct ligand contact versus conformational changes.[29,30] These methods have been applied so far to structured protein−ligand interactions. Here we attempt to extend the domain of applicability of computational methods to an IDP such as AS, by developing an apt computational tool for this class of proteins. This tool uses molecular dynamics (MD) trajectories as input. A comparison between calculated and experimental NMR chemical shifts (CSs) and residual dipolar couplings (RDCs) is used to establish the accuracy of the method. The tool helps in the interpretation of CS changes in 2D ^{1}H−^{15}N NMR spectra (some of which are measured here) on passing from AS to the AS·DOP complex in an aqueous solution.

MATERIALS AND METHODS

Experimental Setup. Plasmid pT7-7 encoding human wild-type AS (courtesy of P. Lansbury, Jr.) was expressed in *Escherichia coli* BL21(DE3) Express grown in M9 minimal medium supplemented with [^{15}N]NH_4Cl (Cambridge Isotopes Laboratories Inc.) as previously described.[31] AS was not N-terminally acetylated. After anion exchange purification, AS was further purified by size exclusion chromatography using a buffer that consisted of 20 mM phosphate and 150 mM NaCl (pH 6.4). Peak fractions corresponding to the monomeric form of the protein were collected and used for NMR measurements. ^{1}H−^{15}N SOFAST−HMQC NMR spectra of AS in the free state and the AS·DOP adduct [dopamine and products of its oxidation cascade formed during the experiment (Figure 1B)] were recorded at 303 K on a Bruker Avance 750 MHz instrument, equipped with cryogenically cooled triple-resonance ^{1}H{^{13}C/^{15}N} TCI probes and z axis self-shielded gradient coils. SOFAST−HMQC pulse sequences were used.[25] The reference spectrum of free AS was recorded on 300 μL of 200 μM uniformly isotope-labeled protein. For NMR measurements of the AS·DOP adduct, 10 mg of dopamine hydrochloride powder (Sigma) was dissolved in the AS solution previously used for the acquisition of the reference spectrum. The final concentration of DOP was 175.8 mM. A decrease in pH resulting from addition of DOP (from 6.4 to 6.2) was corrected with 1 μM NaOH before NMR measurement. Acquisition, processing, and analysis of spectra were performed with TOPSPIN version 2.1 (Bruker) and iNMR version 3.6.3. Mean weighted chemical shift variations (Δcs) per residue read

$$\Delta cs = [(\Delta H)^2 + (\Delta N/10)^2]^{0.5} \quad (1)$$

where Δ indicates the difference between the chemical shift between the bound and free state, given for each backbone amide. Only well-resolved, nonoverlapping AS signals were considered for the analysis.

Computational Methods. *Conformational Indexes.* Recently, we have introduced a quantity that analyzes MD trajectories of folded proteins.[32] This is the so-called cumulative protein angular dispersion index $(PAD_{cum})_{\omega}$, which can be used, along with other quantities, to discriminate between a fluctuating residue and one doing conformational transitions. It is an angular property and varies in the range from 0° to 180°.

Specifically, $(PAD_{cum})_{\omega}$ is defined in terms of the values of Ramachandran angles ψ and Φ of a specific residue of a protein, collected along a MD trajectory:

$$(PAD_{cum})_{\omega} = \frac{180}{\pi} \cos^{-1}\left(\frac{1 - CS_{\bar{\omega}}}{1 + CS_{\bar{\omega}}}\right),$$

where

$$CS_{\bar{\omega}} = \frac{1 - R_{2\bar{\omega}}}{2R_{2\bar{\omega}}},\ R_{k\bar{\omega}} = \frac{1}{N}\left|\sum_{j=1}^{N} e^{ik\bar{\omega}_j}\right| \text{ for } k = 1,2,$$

N is the total number of frames of the MD trajectory, j is a given frame of the trajectory, $\bar{\omega}_j$ is the angle formed by the cumulative vector $\sum_{p=1}^{j} e^{i\omega_p}$, which is the sum of the $e^{i\omega_p}$ vectors occurring in the first j frames and $\omega_p = \psi_p + \phi_p$ (not to be confused with the C_α−C−N−C_α torsion angle in a peptide bond), $NR_{k\bar{\omega}}$ represents the resultant of the N unit vectors $e^{ik\bar{\omega}_j}$, and $CS_{\bar{\omega}}$ is the spread of the $\bar{\omega}_j$ values, which ranges from zero (no dispersion, $R_{1\bar{\omega}} = R_{2\bar{\omega}} = 1$, the vectors $e^{ik\bar{\omega}_j}$ are aligned along a unique direction) to infinity (maximal dispersion, $R_{1\bar{\omega}} = R_{2\bar{\omega}} = 0$, the vectors $e^{ik\bar{\omega}_j}$ are uniformly distributed). $(PAD_{cum})_{\omega}$ increases with the deviations of the $\sum_{p=1}^{j} e^{i\omega_p}$ vectors from the direction of the resultant vector. As an example, let us take a set of six vectors ($e^{i\omega_p}$, where p = 1, 2, ..., 6) associated with fluctuations (Figure 2A) or conformational transitions (Figure

dx.doi.org/10.1021/bi400367r | *Biochemistry* 2013, 52, 6672−6683

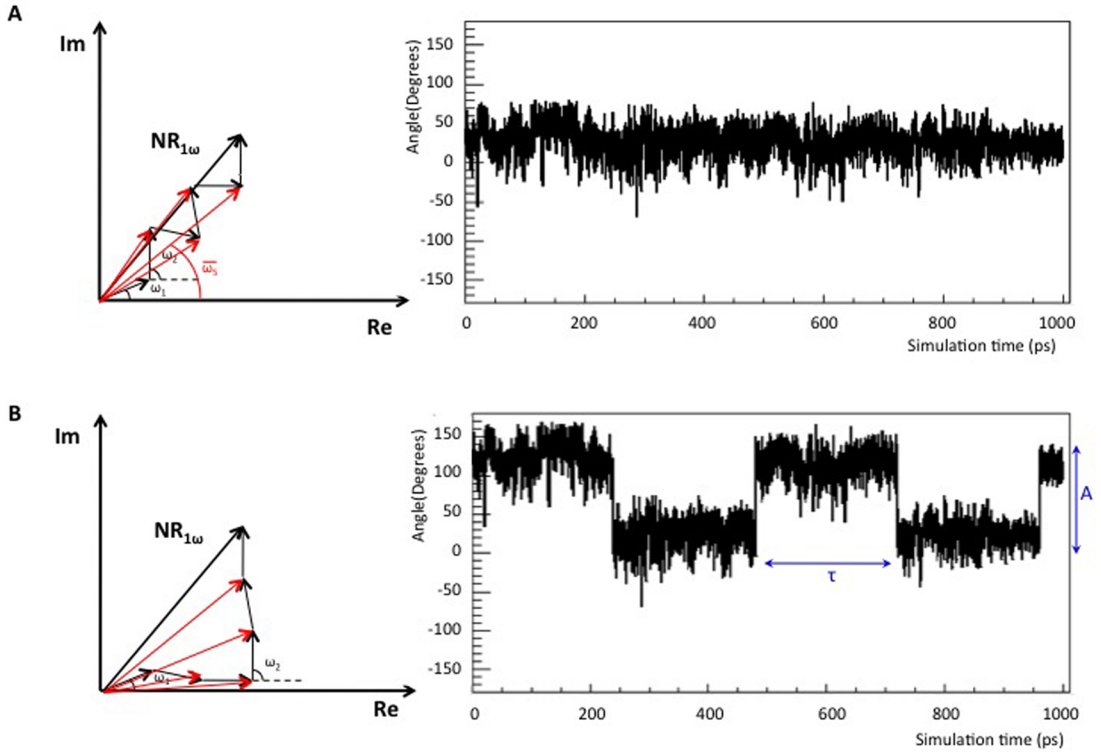

Figure 2. Ramachandran angle representations. On the right are shown values of Ramachandran angle φ of residue M1 of AS, plotted as a function of simulated time in a 1 ns MD simulation (A). Hypothetical transitions of amplitude $A = 120°$ and period $\tau = 200$ ps are introduced (B). On the left are shown representations in the complex plane of $N = 6$ unit vectors $e^{i\omega_p}$ (black) and $e^{i\bar{\omega}_j}$ (red), where the angular ω_p values fluctuate around a given direction (A) and undergo a transition between two perpendicular directions (B). The $e^{i\bar{\omega}_j}$ values are different in panels A and B: they give different values of $(\mathrm{PAD_{cum}})_\omega$, lower for panel A and higher for panel B.

2B), depending on the $e^{i\omega_p}$ vectors' orientations. The $(\mathrm{PAD_{cum}})_\omega$ values in the two cases differ because the corresponding vectors $e^{i\bar{\omega}_j}$ depend on the orientation of the $e^{i\omega_p}$ vectors (see ref 32 for a more extensive discussion).

We next define a new quantity, the transiton amplitude index (TAI_ω), which also varies in the range from 0° to 180° and reads

$$\mathrm{TAI}_\omega = \frac{180}{\pi} \cos^{-1}\left(\frac{1 - \sqrt{\mathrm{CS}_\omega^{\,2} + \mathrm{ATI}_\omega^{\,2}}}{1 + \sqrt{\mathrm{CS}_\omega^{\,2} + \mathrm{ATI}_\omega^{\,2}}}\right)$$

where

$$\mathrm{CS}_\omega = \frac{1 - R_{2\omega}}{2R_\omega};\ R_{k\omega} = \frac{1}{N}\left|\sum_{j=1}^{N} e^{ik\omega_j}\right|$$

and ATI_ω, the so-called angular transition index, discussed in ref 32.

In the next section, by using a numerical example, we show that TAI_ω and $(\mathrm{PAD_{cum}})_\omega$ can be used also for the analysis of IDPs.

Numerical Example. Let us consider the MD trajectory of AS in an aqueous solution, whose total time T is 1 ns. We focus on residue Met1. Φ_i turns out to fluctuate around an average value of 30°, with an amplitude A_0 of 50° and a period τ_0 of 25 ps. We introduce periodic transitions having a period τ and an amplitude A. Through a systematic variation of these two parameters $(A;\tau)$, we observe the following behavior of $(\mathrm{PAD_{cum}})_\omega$ (i) and TAI_ω (ii).

(i) $(\mathrm{PAD_{cum}})_\omega$ is able to discriminate cases in which transitions are dominant from those in which only fluctuations occur (Figure S1A of the Supporting Information). Specifically, when A and τ of the periodic transitions introduced are comparable or smaller than those of the baseline fluctuation ($A \leq A_0$ and $\tau \leq \tau_0$), the $e^{i\bar{\omega}_j}$ vectors' orientations do not (or slightly) deviate from the baseline direction. Hence, index $(\mathrm{PAD_{cum}})_\omega$ assumes small values [<18° in this specific case[b] (see Figure S1A of the Supporting Information)], which is a signature of an angle $\omega_p = \psi_p + \phi_p$ fluctuating. $(\mathrm{PAD_{cum}})_\omega$ has the same response if a single transition occurs, lasting for the majority of total time T (specifically $\tau > {}^3/_4T$). In all the other cases ($A > A_0$ and/or $\tau_0 < \tau < {}^3/_4T$), the $e^{i\bar{\omega}_j}$ vectors' orientations strongly deviate from the baseline direction, which is a signature of an angle $\omega_p = \psi_p + \phi_p$ undergoing transitions. Hence, the $(\mathrm{PAD_{cum}})_\omega$ index assumes larger values [>18° in this specific case (see Figure S1A of the Supporting Information)]. For folded proteins, $(\mathrm{PAD_{cum}})_\omega$ was combined with the protein angular index (PAI).[32] Test calculations show that PAI is not a useful quantity for discriminating between residues fluctuating and making transitions in IDPs (data not shown). It is therefore not used here.

(ii) TAI_ω values are nearly constant when τ varies from 0 to T, and they nearly reproduce the values of parameter A (see Figure S1B of the Supporting Information), except in the case in which the amplitude of the periodic transitions introduced is smaller than the amplitude of the baseline fluctuation ($A < A_0$) or the transitions occur for a negligible fraction of the simulated time ($\tau \ll T$). In these cases, the TAI_ω value approximates the value of the baseline fluctuation amplitude ($\mathrm{TAI}_\omega \approx A_0$).

dx.doi.org/10.1021/bi400367r | *Biochemistry* 2013, 52, 6672−6683

Hence, we conclude that for non-negligible values of A and τ, TAI_ω gives an estimate of A, which is independent of τ.

Computational Details. Our calculations are based on the experimental AS structural ensemble obtained by NMR combined with PRE measurements.[33] AS is not N-terminally acetylated.[34,35] The six representatives of the most-populated clusters used here cover almost three-quarters of the AS conformations in the free nonacetylated form.[17,33,36] The initial configurations of adducts between AS and dopamine and its derivatives in Figure 1B were obtained by docking the ligands onto the six representatives.[17] The minima characterizing these representatives may not dramatically change in the presence of the ligands. Each of the 36 AS·DOP adducts[17] underwent 40 ns of classical molecular dynamics with NAMD version 2.7.[37] The AMBER99SB[38] force field with ILDN modification[39,40] was used to describe the biomolecules and the counterions, and the TIP3P[41] force field was employed for water molecules. The systems were embedded in a water box chosen so that a minimal distance of 10 Å was present between all protein atoms and the edge of the box. The number of water molecules in each box ranged between 76842 and 184638. The overall charge of the system was neutralized by adding nine Na^+ ions. Periodic boundary conditions were applied. During the simulations, the distance between the edge of the box and the nearest atom ranged from ∼10 to ∼25 Å. The distance between an atom and its images turned out to be always greater than ∼17.5 Å (see Table S1 of the Supporting Information). The simulations were performed at 300 K and 1.013 bar by coupling each system with a Langevin thermostat[42] having a coupling coefficient of 5 ps^{-1}, and a Nosé-Hoover Langevin barostat[43] with an oscillation period of 200 fs and a damping time scale of 100 fs. Electrostatic interactions were calculated by using the particle mesh Ewald method.[44] The time step was set to 2 fs. The SHAKE algorithm[45] was applied to fix all bond lengths. We verified the stability and convergence of the trajectories (see Table S2 of the Supporting Information).

Calculated Properties. All the properties reported here were calculated considering only the frames in which DOPs are linked to the protein. Hence, we first detect (i) the persistency of binding (P) here defined as the number of frames in which DOPs form hydrogen bonds (HBs), hydrophobic contacts (HCs), or salt bridges (SBs) with AS, divided by the total number of frames (Table 1). See section S3 and Table S3 of the Supporting Information for details. The following properties were calculated and averaged over the MD trajectories for each configuration of the six adducts. The symbol of average was omitted for the sake of clarity.

Table 1. Persistency of the Formation of DOP Noncovalently Bound to AS in the AS·DOP Representative Conformers (1−6) during the MD Simulations Conducted in This Work

P (%)	DOP	DOPH	DCH	DHI	DQ	IQ
1	40	100	95	68	30	37
2	40	20	100	100	20	100
3	46	100	100	43	30	85
4	22	100	100	100	30	3
5	100	100	100	100	37	100
6	12	65	6	18	30	25

(ii) The percentage of secondary structure elements (SS) was calculated as described in ref 46.

(iii) The end-to-end (E−E) distance was defined as the distance between the N atom of residue Ala140 and the N atom of residue Met1.

(iv) The radius of gyration (R_g) was calculated as

$$R_g = \left(\frac{\sum_i |r_i|^2 m_i}{\sum_i m_i} \right)^{1/2}$$

where m_i is the mass of atom i and r_i the position of C_α atom i respect to the center of mass of the protein.

The following properties were instead averaged over the MD simulations (for AS and AS·DOP) by considering the six configurations altogether. The weight of each configuration in the total average was established by the persistency of binding (P). For these quantities, we use an "over line" to distinguish them from the previously defined quantities, averaged only over the trajectory of the single conformation.

(v) The frequency of AS·DOP HBs and HCs ($\overline{\text{freq}_C}$) was defined as the total number of contacts (n° contacts) of the ith residue in configuration j of AS·DOP

$$\overline{\text{freq}_C} = \frac{100 \frac{\sum_{j=1}^{6} \sum_{i=1}^{n_k} (\text{n° contacts})_{ij}}{n_k}}{\frac{\sum_{j=1}^{6} \sum_{i=1}^{n_{TOT}} (\text{n° contacts})_{ij}}{n_{TOT}}}$$

(vi) The difference $\Delta(\overline{\text{PAD}_{cum}})$ was defined as

$$\Delta(\overline{\text{PAD}_{cum}}) = |(\overline{\text{PAD}_{cum}})_\omega^{\text{AS·DOP}} - (\overline{\text{PAD}_{cum}})_\omega^{\text{AS}}|$$

where $(\overline{\text{PAD}_{cum}})_\omega^{\text{AS·DOP}}$ and $(\overline{PAD_{cum}})_\omega^{\text{AS}}$ are the $(\text{PAD}_{cum})_\omega$ values for the average on AS·DOP adducts and free AS, respectively.

(vii) Chemical Shift and Residual Dipolar Couplings. For AS, we calculated the C, C_α, C_β, and N chemical shifts (CSs) using SHIFTX[47] and H−N residual dipolar couplings (RDCs) using PALES.[48] For AS·DOP, we calculated N CSs with the same methodology.

Statistical Tools. (viii) Statistical Difference between AS and AS·DOP Trajectories. We have demonstrated that TAI_ω is able to quantify the amplitude of the residues' movements. Here, this fact is exploited to distinguish the AS trajectories from the AS·DOP trajectories. We use the multivariate analysis technique.[49]

The TAI_ω values for each of the 140 residues were calculated for the 42 MD trajectories generated in this work (6 × 6 for AS·DOP plus 6 for AS). These values were collected in a 42 × 140 matrix. The matrix underwent a principal component analysis (PCA).[49] We used MultiSpectra.[50] The 95% confidence ellipsis in the score plot of the two principal components was calculated.[51] TAI_ω values were averaged over the residues of the six configurations belonging to the same adduct (TAI_ω').

The p value[51] was calculated for each pair of adducts from the so-called cumulative F distribution function.[51] The p value quantifies the probability of the hypothesis that assumes that AS belongs to the same conformational ensemble of AS·DOP adducts.

(ix) Profile histograms between our measured Δcs (X variable hereafter) and $\Delta(\overline{\text{PAD}_{cum}})$ or $\overline{\text{freq}_C}$ (Y variable hereafter) were calculated as follows. The (X,Y) pairs for each residue were divided into four bins, on the basis of the Δcs values. The size and number of the bins were set to different values for the C-terminal with NAC and N-terminal regions,

dx.doi.org/10.1021/bi400367r | *Biochemistry* 2013, 52, 6672−6683

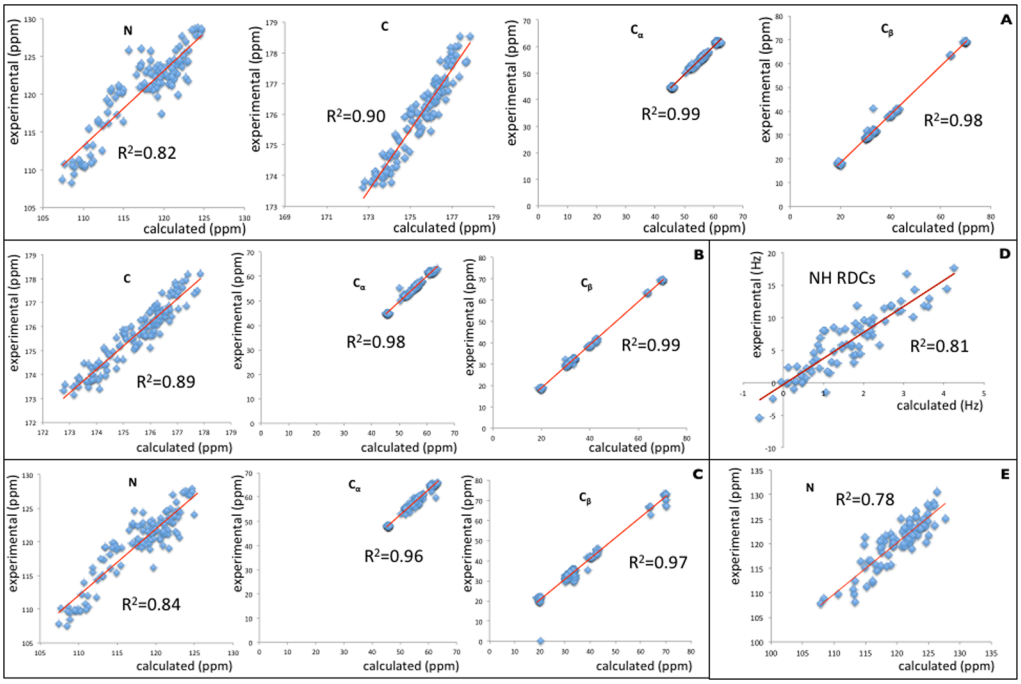

Figure 3. (A–C) Comparison between calculated and experimental CSs of the C, C_α, C_β, and N atoms of AS. Three experimental data sets are considered (from refs 56–58) that were also used in refs 59 and 60. The comparison is with ref 58 in panel A, ref 57 in panel B, and ref 56 in panel C. The data were retrieved from the Biological Magnetic Resonance Data Bank (BMRB):[80] entry 16300 for panel A, entry 6968 for panel B, and entry 17665 for panel C. (D) Comparison between calculated and experimental H–N RDCs of AS. The experimental data set in ref 59 is considered. (E) Comparison between N CSs of AS·DOP calculated from our simulations and experimental CSs measured in this paper.

taking into account the fact that the residues with higher Δcs values belong to the C-terminus and the residues with lower Δcs values belong to the N-terminus. Next, the sample mean of Y ($\langle Y \rangle$) in each bin was plotted against the midpoint of the corresponding Δcs bin. The error for $\langle Y \rangle$ is its standard deviation divided by the number of data pairs that belong to the considered bin. The plots were fit to a trend line.

(x) The Pearson's correlation coefficient (CC)[52] measures the linear dependence between the X and Y variables.

$$\mathrm{CC} = \frac{1}{N-1}\sum_{i=1}^{N}\left(\frac{X_i - \langle X \rangle}{s_X}\right)\left(\frac{Y_i - \langle Y \rangle}{s_Y}\right)$$

where $\langle X \rangle$ and $\langle Y \rangle$ are the sample means and s_X and s_Y are the sample standard deviations of Δcs and $\Delta(\overline{\mathrm{PAD}_{\mathrm{cum}}})$ or $\overline{\mathrm{freq}_{\mathrm{C}}}$, respectively, and N is the sample size, i.e., the number of residues in the considered region.[53] The relative error reads

$$\mathrm{StDev(CC)} = \frac{1-\mathrm{CC}^2}{\sqrt{N-1}}$$

CC ranges from 1 (X and Y are directly correlated) and −1 (Δcs and Y are inversely correlated). If CC = 0, X is not correlated with Y.

(xi) A probability test is performed on the correlation values. We used the Fischer's Z transformation of the CC values,[54] defined as

$$Z = \frac{1}{2}\ln\left(\frac{1+\mathrm{CC}}{1-\mathrm{CC}}\right)$$

with standard deviation

$$\mathrm{StDev}(Z) = \frac{1}{\sqrt{N-3}}$$

Unlike CC, Z follows a normal distribution. It is then possible to calculate its z score,[55] which provides a measure of the distance in standard deviations of the actual Z value from its mean value. The probability of finding a value of Z that is higher than the actual value is given by the area under the normal curve.

RESULTS

MD Simulations. The MD simulations on adducts between AS and dopamine and its derivatives, AS·DOP hereafter [six configurations for six ligands, 36 systems in total (see Figure 1B)], in aqueous solution are an extension of our previous work, reported in ref 17. They are based on AS experimental structural ensembles in aqueous solution obtained by NMR combined with PRE measurements.[33,36] Specifically, we used the six AS configurations representing 73% of the overall experimental population.[17] The initial configurations of the AS·DOP adducts were obtained by docking the six ligands of Figure 1B onto the six AS representatives.[17,c] Here we extend our simulation time to 40 ns for each conformer. Several nonstandard quantities are calculated. For details of these calculations, see Materials and Methods.

Comparison with Experiments and Validation of the Sampling. We compared CSs and RDCs calculated from our simulations on AS with experimental CSs of AS coming from three different experimental data sets from refs 56–58 also used in refs 59 and 60 (Figure 3A–C) and with experimental H–N RDCs of AS in described in ref 59 (Figure 3D). The high correlation between the calculated and experimental CSs (R^2 > 0.8) and between the calculated and experimental RDCs (R^2 ∼ 0.8), shown in Figure 3A–D, validates our models. Comparison between CSs calculated from our simulations of AS·DOP and our corresponding experimental CSs on N atoms also shows a

dx.doi.org/10.1021/bi400367r | Biochemistry 2013, 52, 6672–6683

good correlation ($R^2 \sim 0.8$) (Figure 3E). This points to the reliability of the models of the adducts also.

We conclude that, in spite of the relatively short time scale investigated, our MD simulations of AS and AS·DOP are consistent with NMR data so far reported. This might suggest that the conformations sampled in our MD simulations reproduce to a good extent a significant portion of the experimentally sampled conformations.

Several C-terminal residues, mainly located in the ^{125}YEMPS^{129} region, establish specific HBs and HCs with DOP (Table 2). A graphical representation of the molecular

Table 2. Calculated Frequencies of Hydrogen Bonds (HBs) and Hydrophobic Contacts (HCs) for Specific Regions of the Protein, Averaged over the Six Representative Configurations of AS·DOP, Normalized with Respect to the Number of Residues That Belong to Each Region

	total no. of HBs per residue	total no. of HCs per residue
N-terminus (residues 1−60)	7	6
NAC (residues 61−95)	10	8
C-terminus (residues 96−140)	35	22
YEMPS (residues 125−129)	47	63

details of such interactions is offered in Figure 1C (along with Figures S2 and S3 of the Supporting Information), which report MD snapshots of the adducts between DOP and AS. Our findings are consistent with previously published 2D ^{1}H−^{15}N HSQC spectra,[20] and *in vitro* and *in vivo* experiments,[13,15,17,18] which suggest the presence of noncovalent DOP interactions mainly in the ^{125}YEMPS^{129} sequence.

Ligand binding causes an increase in the overall number of residues involved in secondary structure elements in all the conformers of AS·DOP (Table 3). In particular, the α-helix and β-turn contents increase and the β-sheet content decreases for AS·DOP adducts relative to AS. The decrease in β-sheet content has also been observed in circular dichroism (CD) experiments with AS in the presence of DOP reported in refs 17, 61, and 62. The observed decrease in β-sheet content may reflect the ligands' efficacy in preventing the formation of oligomeric species. A clear trend is instead not identified for the end-to-end distances (Table S4 of the Supporting Information) or R_g (Table S5 of the Supporting Information) of AS·DOP. The average value of R_g of free AS is consistent with structural characterizations of AS with PRE−NMR spectroscopy experiments.[33,36] These studies report an R_g value of 27.2 Å that compares well with our values for the three representatives of the most populated clusters, 24.8 ± 7.4, 28.0 ± 4.1, and 27.5 ± 3.9 Å (Table S5 of the Supporting Information). However, this agreement cannot be taken as a validation. Indeed, several different values of R_g of human AS (at neutral pH and room temperature) have been inferred on the basis of SAXS,[61,63−67] PRE−NMR,[27,33,68,69] and single-molecule FRET[70] experiments. These values range widely, from ∼23 to ∼40 Å (see Figure S4 and Table S6 of the Supporting Information).

NMR Measurements. The changes in NMR chemical shifts upon DOP binding [Δcs, defined in Materials and Methods (Figure 4)] are observed for nearly all AS protein residues. The largest Δcs values are associated with the C-terminus and in particular with the ^{125}YEMPS^{129} region.[d] This result is similar to what was found in reported HSQC spectra.[20]

Table 3. Secondary Structure (SS) Percentage of Six Representative Configurations of AS·DOP and AS (1−6) Averaged over the MD Simulation Time[a]

	SS (%)	1	2	3	4	5	6	average
DOP	α-H	6	4	0	4	3	1	3
	β-s	**0**	**4**	**23**	**0**	**1**	**0**	**5**
	T	24	20	1	23	19	15	17
	BB	1	1	0	2	2	1	1
	TOT	**31**	**29**	**33**	**28**	**24**	**17**	**27**
DOPH	α-H	3	1	2	3	3	2	2
	β-s	**1**	**1**	**0**	**2**	**2**	**1**	**1**
	T	23	20	20	23	14	19	20
	BB	3	2	1	0	0	1	1
	TOT	**30**	**24**	**23**	**28**	**19**	**23**	**25**
DCH	α-H	1	4	7	4	4	3	4
	β-s	**0**	**0**	**0**	**0**	**1**	**1**	**0**
	T	25	20	23	19	16	22	21
	BB	2	1	1	0	2	2	1
	TOT	**28**	**25**	**31**	**24**	**23**	**28**	**26**
DHI	α-H	5	4	1	8	5	1	4
	β-s	**0**	**1**	**4**	**0**	**1**	**1**	**1**
	T	24	16	15	15	21	14	17
	BB	1	2	1	0	2	2	1
	TOT	**30**	**22**	**20**	**27**	**28**	**18**	**24**
DQ	α-H	5	2	3	3	3	3	3
	β-s	**2**	**2**	**2**	**0**	**2**	**0**	**1**
	T	24	18	17	9	11	18	16
	BB	2	2	1	2	3	1	2
	TOT	**32**	**27**	**22**	**14**	**20**	**22**	**23**
IQ	α-H	4	3	3	5	1	2	3
	β-s	**0**	**2**	**0**	**0**	**1**	**1**	**1**
	T	22	14	19	23	15	20	19
	BB	1	0	1	1	2	3	1
	TOT	**27**	**18**	**23**	**29**	**18**	**26**	**23**
AS (no ligand)	α-H	6	2	2	1	2	1	2
	β-s	**1**	**10**	**9**	**1**	**3**	**1**	**4**
	T	17	12	15	11	14	11	13
	BB	2	0	1	3	3	2	2
	TOT	**26**	**24**	**28**	**15**	**21**	**14**	**21**

[a]The total percentage (TOT) and specific secondary structure content (SS) are indicated as α-H (α-helix), β-s (β-sheet), T (turn), and BB (B-bridge). The β-s and TOT content are shown in bold.

We propose here that DOP mainly binds at the C-terminal region, preferentially to the ^{125}YEMPS^{129} residues. Hence, the largest Δcs values observed in the spectra should be mostly caused by noncovalent interactions (i.e., contacts) between AS and the ligands. This hypothesis is fully consistent with MD analysis and available experimental data.[13,15,17,18,20] Moreover, molecular and biochemical approaches, including mutagenesis and competitive binding experiments, also identify the ^{125}YEMPS^{129} region of AS as being crucial in the DOP-induced inhibition of AS fibril formation.[13,15,17,18]

We test our hypothesis by performing a graphical and statistical analysis of Δcs and the frequency of contacts ($\overline{\text{freq}_C}$) between DOP and AS residues during our MD simulations (for a definition of $\overline{\text{freq}_C}$, see Materials and Methods).

The degree of correlation between the Δcs and $\overline{\text{freq}_C}$ is estimated using the Pearson's correlation coefficient (CC)[52] and the statistical z score.[55] The former is defined in a way that when $-1 \leq \text{CC} < 0$ it shows an inverse correlation, while CC =

dx.doi.org/10.1021/bi400367r | *Biochemistry* 2013, 52, 6672−6683

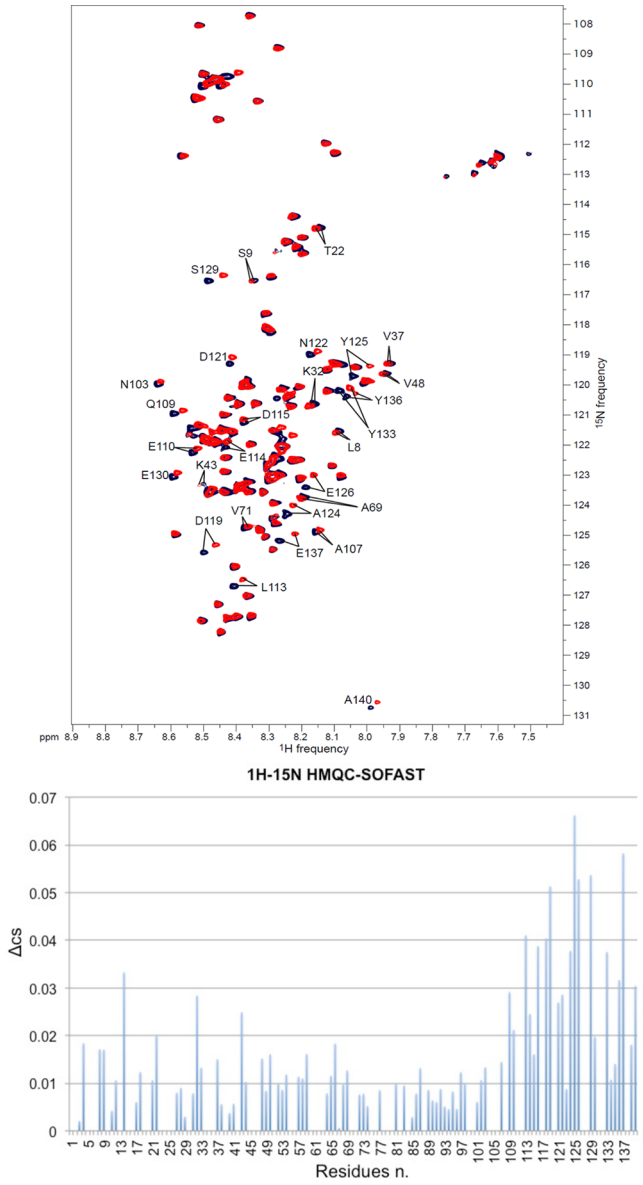

Figure 4. AS NMR chemical shift variation upon addition of DOP. The top panel shows an overlay of $^{1}H-^{15}N$ SOFAST−HMQC spectra of free AS (blue) and AS·DOP (red). Measurements were taken at 303 K on a 200 μM AS sample in a buffer that consisted of 20 mM sodium phosphate and 150 mM NaCl (pH 6.4), with 10 mg of DOP. Well-resolved AS amide resonances that display prominent chemical shift changes upon addition of DOP are shown. The bottom panel shows mean weighted chemical shift changes (Δcs) calculated from NMR spectra.

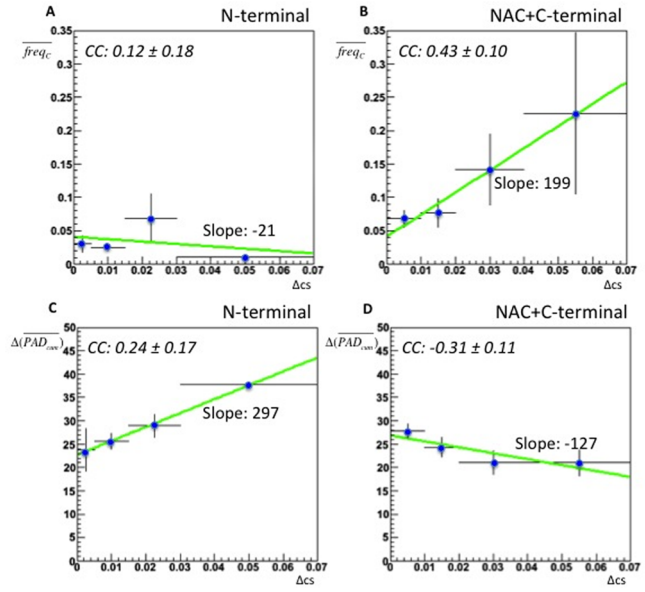

Figure 5. Profile histograms. $\overline{\text{freq}_C}$ (A and B) and $\Delta(\overline{\text{PAD}_{cum}})$ (C and D) are plotted as a function of Δcs for the N-terminal region (residues 1−60, A and C) and the NAC and C-terminal region (residues 61−140, B and D). Each point represents a pair of values: *X* equal to the middle point of the Δcs bin and *Y* equal to the mean value of $\overline{\text{freq}_C}$ (A and B) or $\Delta(\overline{\text{PAD}_{cum}})$ (C and D) calculated on the residues belonging to the corresponding bin. The horizontal lines represent the bin size, and the vertical lines represent the error of the mean value of the *Y* variable (see Materials and Methods). Notice that the last error bar in panel B is larger than the others, because the residues belonging to the last Δcs bin show a high variability in $\overline{\text{freq}_C}$: specifically, the ^{125}YEMPS^{129} residues have the highest values of $\overline{\text{freq}_C}$, but neighbor residues have lower values. Best-fit lines are colored green, and the values of their slopes are reported. The CC values with the relative error for each plot are reported.

0 reveals an absence of correlation and 0 < CC ≤ 1 a direct correlation. The latter ranges between 0 and 100%. The closer the *z* score is to 100%, the higher the probability of a strong correlation between the two quantities. Panels A and B of Figure 5 report the profile histograms between our experimental observable Δcs and $\overline{\text{freq}_C}$ for the N-terminal region and the C-terminal and NAC region, respectively.

Interestingly, $\overline{\text{freq}_C}$ correlates with Δcs in the C-terminal region (Figure 5A,B). The correlation is extended also to the NAC region, but not to the N-terminus. Although the interactions between the DOP and NAC region are minor, some specific residues (i.e., V66, A69, and S87) show significant changes in Δcs (0.018, 0.014, and 0.013 ppm, respectively). These could be caused by specific interaction with DOP (see Figure S3 of the Supporting Information). In the C-terminal and NAC region, the CC value between Δcs and $\overline{\text{freq}_C}$ is positive [CC = 0.43 ± 0.10 (Figure 5B)] and the *z* score is 68% (Table S7 of the Supporting Information). In contrast, the plot between Δcs and $\overline{\text{freq}_C}$ at the N-terminus does not have a defined trend. Consistently, CC is close to zero (Figure 5A,B).

However, few residues with relatively large Δcs values are observed in this region. These include G14, T22, K32, K43, and F4. These residues do not form contacts with the ligands. A visual inspection of the protein conformations during the dynamics led us to suggest (albeit it does not prove) that these Δcs values at the N-terminus might be partially induced by conformational transitions upon DOP binding. DOP was shown to induce conformational changes in AS expressed in neuronal cell lines.[62] Hence, we investigate whether these chemical shift changes are caused, at least in part, by conformational transitions. The latter can be detected with the cumulative protein angular dispersion, $\Delta(\overline{\text{PAD}_{cum}})$ (see Materials and Methods and Figure S5 of the Supporting Information). The higher the $\Delta(\overline{\text{PAD}_{cum}})$, the more the residue experienced conformational rearrangements when passing from the free form to the bound form. Panels C and D of Figure 5 report the profile histograms between our experimental

dx.doi.org/10.1021/bi400367r | *Biochemistry* 2013, 52, 6672−6683

observable Δcs and $\Delta(\overline{PAD_{cum}})$ for the N-terminal region and the C-terminal and NAC region, respectively. $\Delta(\overline{PAD_{cum}})$ and Δcs turned out to be correlated at the N-terminus (Figure 5C). Indeed, both quantities grow evenly, and in addition, the CC is positive [0.24 ± 0.17 (Figure 5C)] and the z score is 60% (Table S7 of the Supporting Information). This indicates a direct correlation between the $\Delta(\overline{PAD_{cum}})$ and Δcs in this region. Therefore, the Δcs at the N-terminus may be induced by conformational transitions upon DOP binding.

Next, we examined the relationship between $\Delta(\overline{PAD_{cum}})$ and Δcs at the C-terminus. The trend line shows a negative slope, and CC is negative. The higher the Δcs values, the lower the $\Delta(\overline{PAD_{cum}})$. This might suggest that the residues involved in the binding have reduced degrees of freedom (Figure 5D).

Other contributions to Δcs may include the interactions of N-terminal residues with weakly populated products of the oxidation cascade of dopamine, as well as the oxidation of the MET residues at positions M1, M5, M116, and M127, due to the long incubation periods with dopamine.[20,71]

Statistical Differences between the Trajectories of AS·DOP′ and AS. The so-called transition amplitude index (TAI_ω), which quantifies the amplitude of motion for each residue (see Materials and Methods), turned out to be larger for AS than for AS·DOP (Table 4 and Figure 6A). A PCA analysis of the TAI_ω values shows that the first principal component (PC1), which captures 24.7% of the total variance[e], separates most AS configurations from the AS·DOP configurations (Figure S6 of the Supporting Information). Graphically, the statistically significant separation is shown by calculating the 95% confidence ellipsis[51] in the score plot of the first two principal components (Figure 6B). The six AS trajectories are well separated from those of AS·DOP (Figure 6B), except for two configurations of the adducts with DOPH and four configurations of the adducts with DCH.

The so-called p value[51] for each pair of residues, which quantifies the probability of the hypothesis that assumes that AS belongs to the same conformational ensemble of AS·DOP adducts, turns out to be <5% (Table 4).

All of this evidence led us to conclude that the spectrum of configurations visited by AS is substantially different from the spectrum of those observed for the AS·DOP adducts. In other words, the MD trajectories of AS·DOP adducts are not a reproduction of free AS trajectories, and they are able to capture the DOP binding effects with a statistical significance.

Table 4. Classification of Results[a]

	DOPH	IQ	DCH	DOP	DHI	DQ	AS (no ligand)
TAI_ω' (deg)	75.1	68.0	89.2	68.7	67.4	67.4	104.3
p value	0.365	0.52	0.158	0.436	0.479	0.494	0.045

[a]TAI_ω values averaged over the residues for each configuration belonging to the same adduct (TAI_ω'); p values for the null hypothesis. See Materials and Methods for details.

DISCUSSION

We have presented a MD-based interpretation of 2D $^1H-^{15}N$ HMQC spectra of AS·DOP adducts. Our analysis leads us to suggest that Δcs at the C-terminus and at few residues in the NAC region (i.e., V66, A69, and S87) may be mostly caused by noncovalent contacts with the ligands, which is consistent with molecular and biochemical approaches[13,15,17,18] and 2D $^1H-^{15}N$ HSQC spectra.[20] We further suggest that the Δcs changes upon binding of DOP at the N-terminus are due, at least in part, to conformational rearrangements of the N-terminal residues. Consistently, DOP was shown to induce conformational changes in AS by fluorescence lifetime imaging microscopy in primary neuronal cultures.[62]

Importantly, the simulations of AS and AS·DOP are significantly different, as shown by a statistical analysis performed here. Notably, they are consistent with the experimental CSs[56−59] and RDCs[59] for AS reported so far as well as with the experimental CS of AS·DOP reported in this

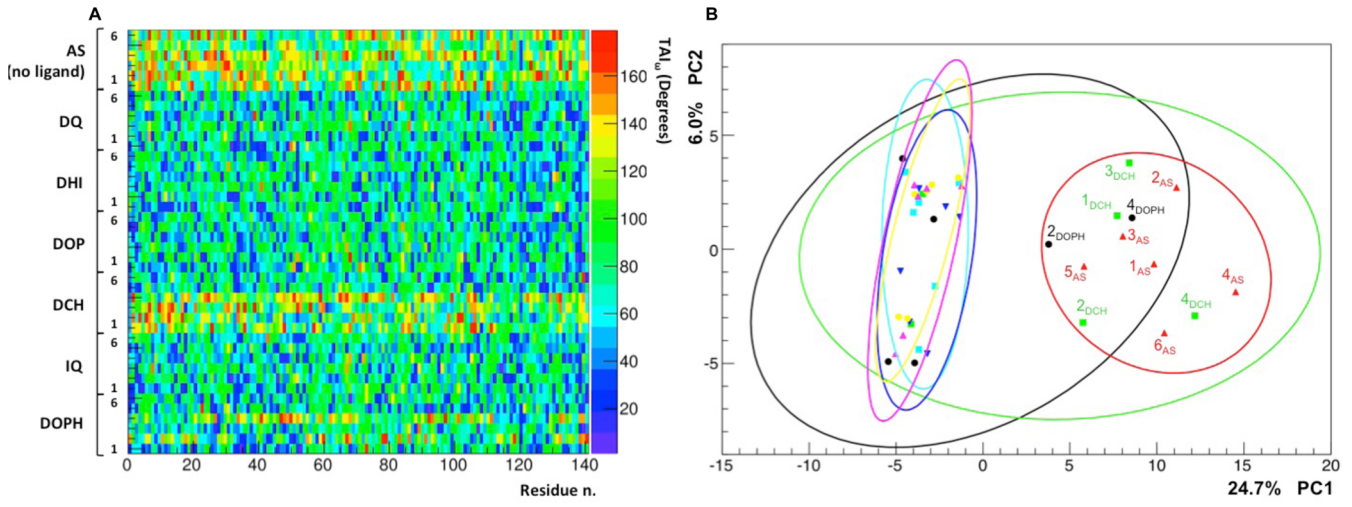

Figure 6. Statistical significance of DOP-induced structural perturbations (A). The TAI_ω values for each residue in AS and AS·DOP (see Materials and Methods for a definition of this quantity) are colored according to their values. The violet color corresponds to the lowest values. The red color corresponds to the highest values. (B) Score plot[51] in the first two principal components of the matrix of the TAI_ω values (PC1 and PC2). The percentage of their variance is reported on the corresponding axis. Each point represents a simulated system. Each group of points has the same color according to the system they represent (either AS or one of the six AS·DOP adducts); 95% confidence ellipses[51] are drawn for each group.

dx.doi.org/10.1021/bi400367r | Biochemistry 2013, 52, 6672−6683

paper. This establishes the quality of our models for the protein both in the free state and in complex with DOP.

Limitations of the Molecular Modeling Procedure. As in any modeling study, the computational procedure presented here has several limitations. First, the performed simulations do not focus on the binding event between AS and DOP, but only the final structural ensemble of the AS·DOP adducts.[17] Second, biomolecular force fields such as AMBER have been constructed for structured proteins, so their domain of applicability to intrinsically unstructured proteins such as AS remains to be established.[39,72,73] However, our current and previous[17] studies seem to suggest that for the specific case of AS, MD simulations with the AMBER99SB force field are able to reproduce the available experimental data. Third, the time scale investigated by simulation of AS and AS·DOP is several orders of magnitude lower than that of NMR and other biophysical experiments to which comparisons have been made. Indeed, with the present computational power, it may be very difficult, if not impossible, to cover with MD the immense conformational space explored by AS in solution if one starts from a random conformation. However, a crucial point here is the fact that our MD simulations are based on AS experimental structural ensembles obtained by NMR combined with PRE measurements.[33,36] This allowed us to use six AS configurations representing 73% of the overall experimental population.[17] Indeed, simulations of these "representative" structures and adducts with small molecules may sample free energy minima associated with conformations not too dissimilar from experimental conformations. In agreement with this hypothesis, our calculations are fully consistent with the available CSs[56−59] and RDCs[59] reported previously. Because of the limited time scale investigated, however, our interpretation of the NMR data can be taken only at the semiquantitative level. Finally, and most importantly, our modeling focuses on one AS molecule interacting with one of the compounds in Figure 1B. However, in the performed experiments, it is not possible to know the DOP derivatives with which the protein interacts. It is presumable that in the experiments one AS protein is interacting simultaneously with more than one oxidation product of dopamine, because its concentration is higher than that of AS. Cooperative effects due to multiple bindings could be present.

In spite of these caveats, the fact that our simulations are consistent with all the available experimental NMR data[56−59] leads us to suggest that key aspects of the interactions between AS and DOP are captured by our study and, therefore, our MD simulations can be of help in interpreting the measured NMR data.

■ ASSOCIATED CONTENT

Ⓢ Supporting Information

Additional data and observations. This material is available free of charge via the Internet at http://pubs.acs.org.

■ AUTHOR INFORMATION

Corresponding Author

*E-mail: g.rossetti@grs-sim.de. Telephone: +49 2461 61 8933.

Notes

The authors declare no competing financial interest.

■ ACKNOWLEDGMENTS

We thank Philipp Selenko's In cell NMR Laboratory (Leibniz Institute of Molecular Pharmacology (FMP Berlin), Department of NMR-supported Structural Biology, Berlin, Germany) for providing us with the NMR spectra and chemical shift values. Computer time provided by the Jülich Supercomputing Center on the JUROPA supercomputer through the allocation of the German Research School for Simulation Sciences is gratefully acknowledged.

■ ABBREVIATIONS

IDP, intrinsically disordered protein; AS, α-synuclein; DOP, dopamine and its derivatives; PD, Parkinson's disease; PRE, paramagnetic relaxation enhancement; 2D NMR, two-dimensional nuclear magnetic resonance; HSQC, heteronuclear single-quantum correlation; HMQC, heteronuclear multiple-quantum correlation; SOFAST, selective optimized-flip-angle short-transient; CS, chemical shift; mwcsv or Δcs, mean weighted chemical shift variation; RDC, residual dipolar coupling; SAXS, small-angle X-ray scattering; FRET, Förster resonance energy transfer; PAI, protein angular index; ATI_{ω}, angular transition index; TAI_{ω}, transition amplitude index; PCA, principal component analysis; $\Delta(\overline{PAD_{cum}})$, cumulative protein angular dispersion index variation; $\overline{freq_C}$, frequency of contacts; HB, hydrogen bond; HC, hydrophobic contact; *P*, persistency of binding; CC, Pearson's correlation coefficient; R_g, radius of gyration; SB, salt bridge.

■ ADDITIONAL NOTES

[a] Also covalent binding may affect fibril formation.[11,14,20,21,74−78]

[b] $(PAD_{cum})_{\omega}$ depends on the amplitude of the intrinsic fluctuations of the residue. For proteins with stable folding, it was found to be 10° (see ref 32); on the other hand, 18° is the amplitude of intrinsic fluctuations for a residues belonging to an IDP.

[c] The 6 ns MD simulations were conducted on each conformer. These turned out to be consistent with a variety of *in vitro* experiments on AS·DOP.[13,15,16] The main results of this previous study are as follows. (i) DOP forms stable contacts to AS and binds to the ^{125}YEMPS^{129} region. (ii) The ligands are further stabilized by long-range electrostatic interactions with glutamate 83 (E83) in the NAC region. (iii) Mutations in the ^{125}YEMPS^{129} region do not affect AS aggregation, which is consistent with the fact that DOP interacts nonspecifically with this region.

[d] The Δcs values of these residues decrease in the following order: Y125, E137, S129, E126, D119, L113, V118, and M116. The relative Δcs values are 1, 0.89, 0.88, 0.79, 0.77, 0.62, 0.60, and 0.58 ppm, respectively.

[e] The second component (PC2) captures the 6% of total variance.

■ REFERENCES

(1) Sung, Y.-h., and Eliezer, D. (2007) Residual Structure, Backbone Dynamics, and Interactions within the Synuclein Family. *J. Mol. Biol.* 372, 689−707.

(2) Fernández, C. O., Hoyer, W., Zweckstetter, M., Jares-Erijman, E. A., Subramaniam, V., Griesinger, C., and Jovin, T. M. (2004) NMR of α-synuclein-polyamine complexes elucidates the mechanism and kinetics of induced aggregation. *EMBO J.* 23, 2039−2046.

(3) Meuvis, J., Gerard, M., Desender, L., Baekelandt, V., and Engelborghs, Y. (2010) The conformation and the aggregation kinetics of α-synuclein depend on the proline residues in its C-terminal region. *Biochemistry 49*, 9345−9352.
(4) Luk, K. C., Kehm, V., Carroll, J., Zhang, B., O'Brien, P., Trojanowski, J. Q., and Lee, V. M. Y. (2012) Pathological α-Synuclein Transmission Initiates Parkinson-like Neurodegeneration in Non-transgenic Mice. *Science 338*, 949−953.
(5) Baba, M., Nakajo, S., Tu, P. H., Tomita, T., Nakaya, K., Lee, V. M., Trojanowski, J. Q., and Iwatsubo, T. (1998) Aggregation of α-synuclein in Lewy bodies of sporadic Parkinson's disease and dementia with Lewy bodies. *Am. J. Pathol. 152*, 879−884.
(6) Spillantini, M. G., Schmidt, M. L., Lee, V. M., Trojanowski, J. Q., Jakes, R., and Goedert, M. (1997) α-Synuclein in Lewy bodies. *Nature 388*, 839−840.
(7) Fearnley, J. M., and Lees, A. J. (1991) Ageing and Parkinson's disease: Substantia nigra regional selectivity. *Brain 114* (Part 5), 2283−2301.
(8) Perez, R. G., Waymire, J. C., Lin, E., Liu, J. J., Guo, F., and Zigmond, M. J. (2002) A Role for α-Synuclein in the Regulation of Dopamine Biosynthesis. *J. Neurosci. 22*, 3090−3099.
(9) Yavich, L., Tanila, H., Vepsäläinen, S., and Jäkälä, P. (2004) Role of α-Synuclein in Presynaptic Dopamine Recruitment. *J. Neurosci. 24*, 11165−11170.
(10) Lehmensiek, V., Tan, E.-M., Schwarz, J., and Storch, A. (2002) Expression of mutant α-synucleins enhances dopamine transporter-mediated MPP+ toxicity in vitro. *NeuroReport 13*, 1279−1283.
(11) Bisaglia, M., Mammi, S., and Bubacco, L. (2007) Kinetic and structural analysis of the early oxidation products of dopamine: Analysis of the interactions with α-synuclein. *J. Biol. Chem. 282*, 15597−15605.
(12) Corona-Avendaño, S., Alarcón-Angeles, G., Rosquete-Pina, G. A., Rojas-Hernández, A., Gutierrez, A., Ramírez-Silva, M. T., Romero-Romo, M., and Palomar-Pardavé, M. (2007) New insights on the nature of the chemical species involved during the process of dopamine deprotonation in aqueous solution: Theoretical and experimental study. *J. Phys. Chem. B 111*, 1640−1647.
(13) Norris, E. H., Giasson, B. I., Hodara, R., Xu, S., Trojanowski, J. Q., Ischiropoulos, H., and Lee, V. M.-Y. (2005) Reversible inhibition of α-synuclein fibrillization by dopaminochrome-mediated conformational alterations. *J. Biol. Chem. 280*, 21212−21219.
(14) Conway, K. A., Rochet, J. C., Bieganski, R. M., and Lansbury, P. T. (2001) Kinetic stabilization of the α-synuclein protofibril by a dopamine-α-synuclein adduct. *Science 294*, 1346−1349.
(15) Mazzulli, J. R., Armakola, M., Dumoulin, M., Parastatidis, I., and Ischiropoulos, H. (2007) Cellular oligomerization of α-synuclein is determined by the interaction of oxidized catechols with a C-terminal sequence. *J. Biol. Chem. 282*, 31621−31630.
(16) Mazzulli, J. R., Mishizen, A. J., Giasson, B. I., Lynch, D. R., Thomas, S. A., Nakashima, A., Nagatsu, T., Ota, A., and Ischiropoulos, H. (2006) Cytosolic catechols inhibit α-synuclein aggregation and facilitate the formation of intracellular soluble oligomeric intermediates. *J. Neurosci. 26*, 10068−10078.
(17) Herrera, F. E., Chesi, A., Paleologou, K. E., Schmid, A., Munoz, A., Vendruscolo, M., Gustincich, S., Lashuel, H. A., and Carloni, P. (2008) Inhibition of α-synuclein fibrillization by dopamine is mediated by interactions with five C-terminal residues and with E83 in the NAC region. *PLoS One 3*, e3394.
(18) Latawiec, D., Herrera, F. E., Bek, A., Losasso, V., Candotti, M., Benetti, F., Carlino, E., Kranjc, A., Lazzarino, M., Gustincich, S., Carloni, P., and Legname, G. (2010) Modulation of α-synuclein aggregation by dopamine analogs. *PLoS One 5*, e9234.
(19) Li, H.-T., Lin, D.-H., Luo, X.-Y., Zhang, F., Ji, L.-N., Du, H.-N., Song, G.-Q., Hu, J., Zhou, J.-W., and Hu, H.-Y. (2005) Inhibition of α-synuclein fibrillization by dopamine analogs via reaction with the amino groups of α-synuclein. Implication for dopaminergic neurodegeneration. *FEBS J. 272*, 3661−3672.
(20) Bisaglia, M., Tosatto, L., Munari, F., Tessari, I., de Laureto, P. P., Mammi, S., and Bubacco, L. (2010) Dopamine quinones interact with α-synuclein to form unstructured adducts. *Biochem. Biophys. Res. Commun. 394*, 424−428.
(21) Chary, K. V. R., and Govil, G. (2008) *NMR in Biological Systems, From Molecules to Humans*, Vol. 6 (electronic reproduction), Springer, Dordrecht, The Netherlands.
(22) Rezaei-Ghaleh, N., Blackledge, M., and Zweckstetter, M. (2012) Intrinsically Disordered Proteins: From Sequence and Conformational Properties toward Drug Discovery. *ChemBioChem 13*, 930−950.
(23) Schanda, P., and Brutscher, B. (2005) Very Fast Two-Dimensional NMR Spectroscopy for Real-Time Investigation of Dynamic Events in Proteins on the Time Scale of Seconds. *J. Am. Chem. Soc. 127*, 8014−8015.
(24) Kiefhaber, T., Bachmann, A., and Jensen, K. S. (2012) Dynamics and mechanisms of coupled protein folding and binding reactions. *Curr. Opin. Struct. Biol. 22*, 21−29.
(25) Schanda, P., Kupče, Ē., and Brutscher, B. (2005) SOFAST-HMQC Experiments for Recording Two-dimensional Heteronuclear Correlation Spectra of Proteins within a Few Seconds. *J. Biomol. NMR 33*, 199−211.
(26) Mukrasch, M. D., Bibow, S., Korukottu, J., Jeganathan, S., Biernat, J., Griesinger, C., Mandelkow, E., and Zweckstetter, M. (2009) Structural polymorphism of 441-residue tau at single residue resolution. *PLoS Biol. 7*, e34.
(27) Salmon, L., Nodet, G., Ozenne, V., Yin, G., Jensen, M. R., Zweckstetter, M., and Blackledge, M. (2010) NMR characterization of long-range order in intrinsically disordered proteins. *J. Am. Chem. Soc. 132*, 8407−8418.
(28) Wishart, D. S., and Nip, A. M. (1998) Protein chemical shift analysis: A practical guide. *Biochem. Cell Biol. 76*, 153−163.
(29) Selvaratnam, R., Chowdhury, S., VanSchouwen, B., and Melacini, G. (2011) Mapping allostery through the covariance analysis of NMR chemical shifts. *Proc. Natl. Acad. Sci. U.S.A. 108*, 6133−6138.
(30) Selvaratnam, R., VanSchouwen, B., Fogolari, F., Mazhab-Jafari, M. T., Das, R., and Melacini, G. (2012) The projection analysis of NMR chemical shifts reveals extended EPAC autoinhibition determinants. *Biophys. J. 102*, 630−639.
(31) Hoyer, W., Antony, T., Cherny, D., Heim, G., Jovin, T. M., and Subramaniam, V. (2002) Dependence of α-Synuclein Aggregate Morphology on Solution Conditions. *J. Mol. Biol. 322*, 383−393.
(32) Caliandro, R., Rossetti, G., and Carloni, P. (2012) Local Fluctuations and Conformational Transitions in Proteins. *J. Chem. Theory Comput. 8*, 4775−4785.
(33) Dedmon, M. M., Lindorff-Larsen, K., Christodoulou, J., Vendruscolo, M., and Dobson, C. M. (2005) Mapping Long-Range Interactions in α-Synuclein using Spin-Label NMR and Ensemble Molecular Dynamics Simulations. *J. Am. Chem. Soc. 127*, 476−477.
(34) Maltsev, A. S., Ying, J., and Bax, A. (2012) Impact of N-Terminal Acetylation of α-Synuclein on Its Random Coil and Lipid Binding Properties. *Biochemistry 51*, 5004−5013.
(35) Trexler, A. J., and Rhoades, E. (2012) N-terminal acetylation is critical for forming α-helical oligomer of α-synuclein. *Protein Sci. 21*, 601−605.
(36) Losasso, V., Pietropaolo, A., Zannoni, C., Gustincich, S., and Carloni, P. (2011) Structural Role of Compensatory Amino Acid Replacements in the α-Synuclein Protein. *Biochemistry 50*, 6994−7001.
(37) Phillips, J. C., Braun, R., Wang, W., Gumbart, J., Tajkhorshid, E., Villa, E., Chipot, C., Skeel, R. D., Kalé, L., and Schulten, K. (2005) Scalable molecular dynamics with NAMD. *J. Comput. Chem. 26*, 1781−1802.
(38) Hornak, V., Abel, R., Okur, A., Strockbine, B., Roitberg, A., and Simmerling, C. (2006) Comparison of multiple Amber force fields and development of improved protein backbone parameters. *Proteins 65*, 712−725.
(39) Lindorff-Larsen, K., Piana, S., Palmo, K., Maragakis, P., Klepeis, J. L., Dror, R. O., and Shaw, D. E. (2010) Improved side-chain torsion potentials for the Amber ff99SB protein force field. *Proteins 78*, 1950−1958.

(40) Lindorff-Larsen, K., Maragakis, P., Piana, S., Eastwood, M. P., Dror, R. O., and Shaw, D. E. (2012) Systematic validation of protein force fields against experimental data. *PLoS One 7*, e32131.
(41) Jorgensen, W., Chandrasekhar, J., Madura, J., Impey, R., and Klein, M. (1983) Comparison of simple potential functions for simulating liquid water. *J. Chem. Phys. 79*, 926−935.
(42) Adelman, S., and Doll, J. (1976) Generalized Langevin equation approach for atom-solid-surface scattering. General formulation for classical scattering of harmonic solids. *J. Chem. Phys. 64*, 2375−2388.
(43) Feller, S., Zhang, Y., Pastor, R., and Brooks, B. (1995) Constant pressure molecular dynamics simulation. The Langevin piston method. *J. Chem. Phys. 103*, 4613−4621.
(44) Darden, T., York, D., and Pedersen, L. (1993) Particle mesh Ewald: An N-log(N) method for Ewald sums in large systems. *J. Chem. Phys. 98*, 10089−10092.
(45) Ryckaert, J., Ciccotti, G., and Berendsen, H. (1977) Numerical integration of cartesian equations of motion of a system with constraints. Molecular dynamics of N-alkanes. *J. Comput. Phys. 23*, 327−341.
(46) Humphrey, W., Dalke, A., and Schulten, K. (1996) VMD: Visual molecular dynamics. *J. Mol. Graphics 14*, 33−38.
(47) Neal, S., Nip, A., Zhang, H., and Wishart, D. (2003) Rapid and accurate calculation of protein ^{1}H, ^{13}C and ^{15}N chemical shifts. *J. Biomol. NMR 26*, 215−240.
(48) Zweckstetter, M. (2008) NMR: Prediction of molecular alignment from structure using the PALES software. *Nat. Protoc. 3*, 679−690.
(49) Wold, S., Esbensen, K., and Geladi, P. (1987) Principal component analysis. *Chemom. Intell. Lab. 2*, 37−52.
(50) Caliandro, R., Di Profio, G., and Nicolotti, O. (2013) Multivariate analysis of quaternary carbamazepine-saccharin mixtures by X-ray diffraction and infrared spectroscopy. *J. Pharm. Biomed. Anal. 78−79*, 269−279.
(51) Worley, B., Halouska, S., and Powers, R. (2013) Utilities for quantifying separation in PCA/PLS-DA scores plots. *Anal. Biochem. 433*, 102−104.
(52) Lee Rodgers, J., and Nicewander, W. A. (1988) Thirteen Ways to Look at the Correlation Coefficient. *Am. Stat. 42*, 59−66.
(53) Hotelling, H. (1953) New Light on the Correlation Coefficient and its Transforms. *Journal of the Royal Statistical Society. Series B (Methodological) 15*, 193−232.
(54) Fang, F. C., Steen, R. G., and Casadevall, A. (2012) Misconduct accounts for the majority of retracted scientific publications. *Proc. Natl. Acad. Sci. U.S.A. 109*, 17028−17033.
(55) Altman, E. I. (1968) Financial Ratios, Discriminant Analysis and the Prediction of Corporate Bankruptcy. *Journal of Finance 23* (No. 4), 589−609.
(56) Wang, W., Perovic, I., Chittuluru, J., Kaganovich, A., Nguyen, L. T. T., Liao, J., Auclair, J. R., Johnson, D., Landeru, A., Simorellis, A. K., Ju, S., Cookson, M. R., Asturias, F. J., Agar, J. N., Webb, B. N., Kang, C., Ringe, D., Petsko, G. A., Pochapsky, T. C., and Hoang, Q. Q. (2011) A soluble α-synuclein construct forms a dynamic tetramer. *Proc. Natl. Acad. Sci. U.S.A. 108*, 17797−17802.
(57) Bermel, W., Bertini, I., Felli, I. C., Lee, Y.-M., Luchinat, C., and Pierattelli, R. (2006) Protonless NMR Experiments for Sequence-Specific Assignment of Backbone Nuclei in Unfolded Proteins. *J. Am. Chem. Soc. 128*, 3918−3919.
(58) Rao, J. N., Kim, Y. E., Park, L. S., and Ulmer, T. S. (2009) Effect of pseudorepeat rearrangement on α-synuclein misfolding, vesicle binding, and micelle binding. *J. Mol. Biol. 390*, 516−529.
(59) Gurry, T., Ullman, O., Fisher, C. K., Perovic, I., Pochapsky, T., and Stultz, C. M. (2013) The Dynamic Structure of α-Synuclein Multimers. *J. Am. Chem. Soc. 135*, 3865−3872.
(60) Ullman, O., Fisher, C. K., and Stultz, C. M. (2011) Explaining the Structural Plasticity of α-Synuclein. *J. Am. Chem. Soc. 133*, 19536−19546.
(61) Rekas, A., Knott, R., Sokolova, A., Barnham, K., Perez, K., Masters, C., Drew, S., Cappai, R., Curtain, C., and Pham, C. L. (2010) The structure of dopamine induced α-synuclein oligomers. *Eur. Biophys. J. 39*, 1407−1419.
(62) Outeiro, T. F., Klucken, J., Bercury, K., Tetzlaff, J., Putcha, P., Oliveira, L. M. A., Quintas, A., McLean, P. J., and Hyman, B. T. (2009) Dopamine-Induced Conformational Changes in α-Synuclein. *PLoS One 4*, e6906.
(63) Binolfi, A., Rasia, R. M., Bertoncini, C. W., Ceolin, M., Zweckstetter, M., Griesinger, C., Jovin, T. M., and Fernandez, C. O. (2006) Interaction of α-Synuclein with Divalent Metal Ions Reveals Key Differences: A Link between Structure, Binding Specificity and Fibrillation Enhancement. *J. Am. Chem. Soc. 128*, 9893−9901.
(64) Uversky, V. N. (2001) Evidence for a Partially Folded Intermediate in α-Synuclein Fibril Formation. *J. Biol. Chem. 276*, 10737−10744.
(65) Tashiro, M., Kojima, M., Kihara, H., Kasai, K., Kamiyoshihara, T., Uéda, K., and Shimotakahara, S. (2008) Characterization of fibrillation process of α-synuclein at the initial stage. *Biochem. Biophys. Res. Commun. 369*, 910−914.
(66) Li, J., Uversky, V. N., and Fink, A. L. (2001) Effect of Familial Parkinson's Disease Point Mutations A30P and A53T on the Structural Properties, Aggregation, and Fibrillation of Human α-Synuclein. *Biochemistry 40*, 11604−11613.
(67) Uversky, V. N., Li, J., Souillac, P., Millett, I. S., Doniach, S., Jakes, R., et al. (2002) Biophysical properties of the synucleins and their propensities to fibrillate: Inhibition of α-synuclein assembly by β- and γ-synucleins. *J. Biol. Chem. 277*, 11970−11978.
(68) Cho, M. K., Nodet, G., Kim, H. Y., Jensen, M. R., Bernado, P., Fernandez, C. O., Becker, S., Blackledge, M., and Zweckstetter, M. (2009) Structural characterization of α-synuclein in an aggregation prone state. *Biophys. J. 18*, 1840−1846.
(69) Bertoncini, C. W., Jung, Y. S., Fernandez, C. O., Hoyer, W., Griesinger, C., Jovin, T. M., and Zweckstetter, M. (2005) Release of long-range tertiary interactions potentiates aggregation of natively unstructured α-synuclein. *Proc. Natl. Acad. Sci. U.S.A. 102*, 1430−1435.
(70) Nath, A., Sammalkorpi, M., DeWitt, D. C., Trexler, A. J., Elbaum-Garfinkle, S., O'Hern, C. S., and Rhoades, E. (2012) The Conformational Ensembles of α-Synuclein and Tau: Combining Single-Molecule FRET and Simulations. *Biophys. J. 103*, 1940−1949.
(71) Nakaso, K., Tajima, N., Ito, S., Teraoka, M., Yamashita, A., Horikoshi, Y., Kikuchi, D., Mochida, S., Nakashima, K., and Matsura, T. (2013) Dopamine-mediated oxidation of methionine 127 in α-synuclein causes cytotoxicity and oligomerization of α-synuclein. *PLoS One 8*, e55068.
(72) Click, T. H., Ganguly, D., and Chen, J. (2010) Intrinsically Disordered Proteins in a Physics-Based World. *Int. J. Mol. Sci. 11*, 5292−5309.
(73) Nerenberg, P. S., and Head-Gordon, T. (2011) Optimizing Protein−Solvent Force Fields to Reproduce Intrinsic Conformational Preferences of Model Peptides. *J. Chem. Theory Comput. 7*, 1220−1230.
(74) Ito, S., Kato, T., and Fujita, K. (1988) Covalent binding of catechols to proteins through the sulphydryl group. *Biochem. Pharmacol. 37*, 1707−1710.
(75) Hastings, T. G., Lewis, D. A., and Zigmond, M. J. (1996) Role of oxidation in the neurotoxic effects of intrastriatal dopamine injections. *Proc. Natl. Acad. Sci. U.S.A. 93*, 1956−1961.
(76) Kuhn, D. M., Arthur, R. E., Thomas, D. M., and Elferink, L. A. (1999) Tyrosine Hydroxylase Is Inactivated by Catechol-Quinones and Converted to a Redox-Cycling Quinoprotein. *J. Neurochem. 73*, 1309−1317.
(77) Whitehead, R. E., Ferrer, J. V., Javitch, J. A., and Justice, J. B. (2001) Reaction of oxidized dopamine with endogenous cysteine residues in the human dopamine transporter. *J. Neurochem. 76*, 1242−1251.
(78) LaVoie, M. J., Ostaszewski, B. L., Weihofen, A., Schlossmacher, M. G., and Selkoe, D. J. (2005) Dopamine covalently modifies and functionally inactivates parkin. *Nat. Med. 11*, 1214−1221.

(79) Wallace, A. C., Laskowski, R. A., and Thornton, J. M. (1995) LIGPLOT: A program to generate schematic diagrams of protein-ligand interactions. *Protein Eng. 8*, 127−134.
(80) Ulrich, E. L., Akutsu, H., Doreleijers, J. F., Harano, Y., Ioannidis, Y. E., Lin, J., Livny, M., Mading, S., Maziuk, D., Miller, Z., Nakatani, E., Schulte, C. F., Tolmie, D. E., Kent Wenger, R., Yao, H., and Markley, J. L. (2008) BioMagResBank. *Nucleic Acids Res. 36*, D402−D408.